

# Density functional study of $\alpha$ -CrCl<sub>2</sub>: Structural, electronic, and magnetic properties

A. Hermann,<sup>1,\*</sup> B. Vest,<sup>1</sup> and P. Schwerdtfeger<sup>1,†</sup>

<sup>1</sup>*Centre of Theoretical Chemistry and Physics, Institute of Fundamental Sciences, Massey University (Auckland Campus), Private Bag 102904 North Shore MSC, New Zealand*

(Received 21 August 2006; revised manuscript received 3 October 2006; published 4 December 2006)

We present *first-principles* density functional calculations (DFT) on the  $\alpha$  phase solid state of the transition metal dihalide compound CrCl<sub>2</sub>. Structural parameters are optimized using local spin density approximation (LSDA) and semilocal generalized gradient approximation (GGA) exchange-correlation functionals. Different magnetic coupling schemes are investigated. In agreement with experiment we find that  $\alpha$ -CrCl<sub>2</sub> forms anti-ferromagnetically coupled chains that are connected via weaker Cr-Cl bonds. The internal crystal parameters are well described within DFT-GGA. The absorption spectrum near the onset is dominated by spin-allowed transitions between neighboring Cr atoms. Magnetic coupling constants are calculated from symmetry-breaking solutions of the electronic Hamiltonian. Several DFT-based methods are benchmarked with respect to their ability to reproduce the experimental coupling constants. Both LSDA and GGA fail to do so, and the inclusion of exact exchange worsens the results. Introducing a suitable onsite repulsion term yields good agreement with experiment.

DOI: 10.1103/PhysRevB.74.224402

PACS number(s): 75.50.Ee, 71.20.-b, 71.15.Mb

## I. INTRODUCTION

The accurate theoretical description of materials in the solid state is a longstanding goal of solid state physics and chemistry. Over the last decades, density functional theory (DFT) has emerged as the method of choice to describe structural and electronic properties of insulators, semiconductors, and metals. There are, however, certain shortcomings within common implementations of DFT that limit its accuracy, which originate in the local or semilocal description of the electronic exchange-correlation energy. Several methodological attempts have been made to overcome DFT's deficiencies in one way or another: the introduction of self-interaction correction (SIC) terms to the electronic Hamiltonian to better describe localized states;<sup>1</sup> the implementation of a Hubbard-Hamiltonian atop DFT local spin density approximations (LSDA+U) to account for onsite repulsion energies of partially filled *d* or *f* shells;<sup>2</sup> the inclusion of explicit van der Waals corrections for weakly bonded systems;<sup>3</sup> the partial inclusion of the exact exchange operator either applied directly to the Kohn-Sham orbitals<sup>4,5</sup> or as part of an optimized effective potential.<sup>6,7</sup>

A particularly challenging field is the correct description of magnetic properties of transition-metal compounds. We investigate the performance of DFT and several of the above-mentioned extensions for predicting the magnetic coupling constants of  $\alpha$ -CrCl<sub>2</sub>, an insulating transition metal dihalide. We show that the generalized gradient approximations (GGA) of the exchange-correlation energy<sup>8,9</sup> give the best results among the parameter-free methods. However, even then the coupling constants are overestimated by a factor of two. Including exact exchange worsens the results drastically, giving qualitatively wrong results. By adjusting the U constant in a LSDA+U approach good agreement with experiment can be achieved.

The investigation of the gas phase properties of the first row transition metal halides is an active area of research in both experimental and theoretical chemistry.<sup>10</sup> The combina-

tion of a partially filled 3*d* subshell along with significant 4*s*-3*d* orbital mixing gives rise to many low-lying, closely spaced energy states for the chromium dihalides. The correct description of these spin states by density functional theory is currently a nontrivial task. It is however, also difficult to determine the linearity of CrCl<sub>2</sub> in the gas phase due to the presence of extra absorption peaks arising from the vibrations of the clusters in matrix isolation infrared spectroscopy.<sup>11,12</sup> Several *ab initio* and DFT calculations have been performed on the gas phase, monomeric form of the chromium dihalides with promising results.<sup>13-17</sup> An accurate calculation of the ground state properties of the CrCl<sub>2</sub> monomer needs to include a thorough calculation of the correlation energy. This is because the energy gap between the ground state and first excited state is only around 0.5 eV.<sup>14</sup> For example, unrestricted Hartree-Fock (UHF) calculations by Hillier *et al.*<sup>18</sup> incorrectly predict the ground state of CrCl<sub>2</sub> to be the <sup>5</sup>Σ<sub>g</sub><sup>+</sup> state. It is assumed that the dimeric form of the chromium dihalides is of D<sub>2h</sub> symmetry, antiferromagnetically coupled,<sup>10,17</sup> and consists of two CrCl<sub>2</sub> units bonded together by two Cl bridging the Cr atoms. This structure is quite similar to the building block of the two-dimensional chains of CrCl<sub>2</sub> molecules found in the  $\alpha$  phase of crystalline CrCl<sub>2</sub>.<sup>19,20</sup> However, there is no experimental and/or theoretical evidence that supports the predicted structure of Cr<sub>2</sub>Cl<sub>4</sub>, and there are no theoretical calculations to date predicting the properties of crystalline CrCl<sub>2</sub>. Therefore, calculations on the solid phase of  $\alpha$ -CrCl<sub>2</sub> will not only provide valuable geometric information on CrCl<sub>2</sub>, but will also allow one to determine the energetic consequences of various coupling schemes within and among the chains of CrCl<sub>2</sub>.

## II. METHOD

To calculate the ground state properties of  $\alpha$ -CrCl<sub>2</sub>, we employ density functional theory (DFT) in conjunction with a plane wave basis set as implemented in the Vienna *Ab initio* Simulation Package.<sup>21</sup> The electron-electron interac-

tion is modeled using the local spin density approximation<sup>22,23</sup> (LSDA) or the generalized gradient approximation (GGA) by Perdew *et al.*<sup>8</sup> (PW91) of the exchange-correlation energy. The electron-ion interaction is modeled using the projector augmented wave (PAW) method,<sup>24,25</sup> which on one hand gives access to the all-electron wave functions in the atomic core regions, but on the other hand allows one to restrict the expansion of the electronic wave functions to a rather moderate cutoff of 450 eV in the present case. Brillouin zone (BZ) integrations are carried out on a regular mesh in reciprocal space, equivalent to 128  $\mathbf{k}$  points in the BZ of the primitive  $\alpha$ -CrCl<sub>2</sub> unit cell. To find the minimal energy structure within DFT-LSDA/GGA, we optimize the cell lattice vectors and all internal coordinates for a number of given cell volumes, using a conjugate-gradient or quasi-Newton algorithm to minimize the Hellmann-Feynman forces. We consider a structure to be in equilibrium if each Cartesian component of the atomic forces is below 5 meV/Å. We fit the resulting  $E(V)$  curve with a Vinet equation of state (EOS),<sup>26</sup> and finally optimize the cell parameters and internal structure at the equilibrium cell volume  $V_0$ .

### III. STRUCTURAL RESULTS

Crystalline  $\alpha$ -CrCl<sub>2</sub> has an orthorhombic unit cell and  $Pnmm$  space group symmetry.<sup>19,20</sup> Every Cr atom is surrounded by an elongated and distorted octahedron of Cl atoms, see Fig. 1. Four of these form a rectangle with the Cr atom in its center, the remaining two being farther away, approximately perpendicular to the rectangular plane. Edge-connected rectangles and their embedded Cr atoms form CrCl<sub>2</sub> chains along the crystallographic  $c$  axis. The spins of the Cr 3d electrons are experimentally found to be coupled antiferromagnetically along these chains.<sup>27,28</sup>

We want to study ferromagnetic (FM) and antiferromagnetic (AFM) coupling along the chains (note that the  $\alpha$ -CrCl<sub>2</sub> crystal is always an antiferromagnet; our notion refers only to the intrachain coupling). To this end we fix the initial magnetic moments of the Cr atoms in the unit cell accordingly. Note that the AFM unit cell is twice as long along the  $c$  direction as the FM unit cell. Figure 1 shows the magnetic unit cell of  $\alpha$ -CrCl<sub>2</sub>, together with some of the surrounding atoms in neighboring cells to illustrate the chain structure.

Table I compiles the experimental and our theoretical results on the structural properties of  $\alpha$ -CrCl<sub>2</sub>. The theoretical values include LSDA and PW91 results for both the FM and AFM magnetic coupling. Additionally, Fig. 2 shows the plots of the binding energy  $E_0$  per CrCl<sub>2</sub> molecule vs the volume  $\Omega_0$  per molecule and their fits with an EOS. From Table I we see that the unit cell parameters do not depend very much on the magnetic structure of the crystal. However, Fig. 2 shows that the AFM alignment along the crystal  $c$  axis is energetically clearly favored, using both LSDA and PW91. Further, we find an overbinding effect in LSDA perpendicular to the  $c$  axis, underestimating the experimental lattice constants by about 6–8%. Within PW91, however, we get a slightly under-bonded structure, having the  $a$  and  $b$  lattice constants overestimated by about 5%. For the  $c$  direction, both meth-

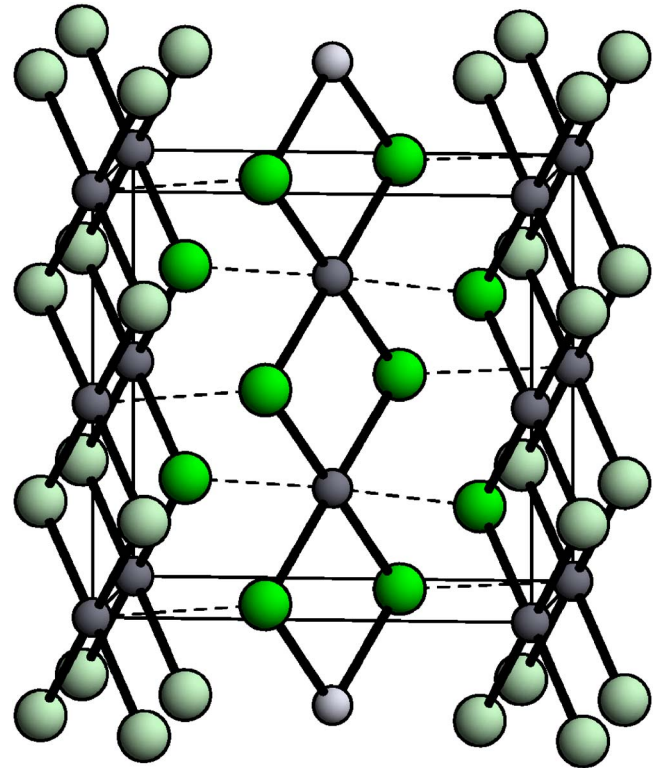


FIG. 1. (Color online) Magnetic unit cell of antiferromagnetically coupled  $\alpha$ -CrCl<sub>2</sub>, with surrounding atoms to emphasize the chain structure. Green/large (gray/small) spheres denote Cl (Cr) atoms. Dashed lines indicate elongated octahedral bonds.

ods yield values lower than the experimental value, with PW91 showing the smaller deviations. Thus, the theoretical unit cell volume for the AFM structure is 8% larger (17% smaller) within PW91 (LSDA) than the experimental value. We conclude that DFT-GGA using the PW91 functional is suitable to describe the structural properties of  $\alpha$ -CrCl<sub>2</sub>, whereas DFT-LSDA overestimates the bond strengths within the crystal significantly.

The Cr and Cl atoms are located at the Wyckoff positions  $2b$  and  $4g$ , respectively. The  $4g$  parameters  $x$  and  $y$ , the Cr-Cl bond lengths and the octahedron distortion angle  $\delta$  are given in Table II. There, we refer to “Cl<sub>(1)</sub>” or “Cl<sub>(2)</sub>” atoms

TABLE I. Structural data of  $\alpha$ -CrCl<sub>2</sub>-unit cell: experimental and theoretical lattice constants. AFM unit cell is twice as long in  $c$  direction as FM unit cell.

	$a_0$ (Å)	$b_0$ (Å)	$c_0$ (Å)
Tracy <i>et al.</i> <sup>a</sup>	6.653	5.992	3.494
Oswald <sup>b</sup>	6.624	5.974	3.488
FM, DFT-PW91 <sup>c</sup>	7.077	6.323	3.451
FM, DFT-LSDA	6.081	5.585	3.349
AFM, DFT-PW91 <sup>c</sup>	7.038	6.321	6.801
AFM, DFT-LSDA	6.077	5.643	6.698

<sup>a</sup>Reference 20.

<sup>b</sup>Reference 19.

<sup>c</sup>Reference 8.

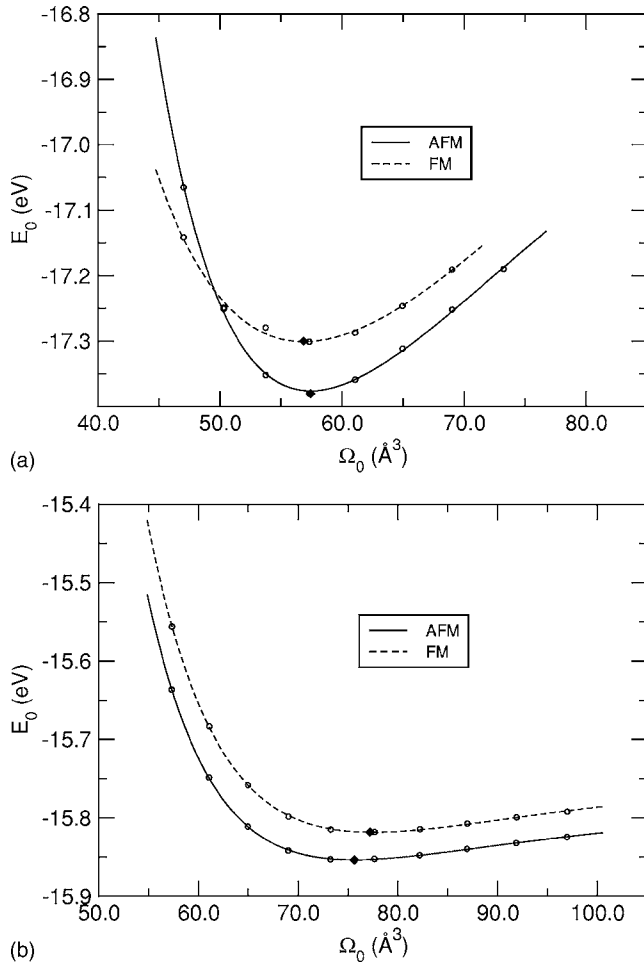


FIG. 2.  $E(\Omega_0)$ -curves. Circles: data points, lines: Vinet-fit, diamonds: parameters of final structure. Upper panel: DFT-LSDA calculation; lower panel: DFT-PW91 calculation.  $E_0$ : binding energy per CrCl<sub>2</sub> unit,  $\Omega_0$ : unit cell volume per CrCl<sub>2</sub> unit.

as atoms within the same chain or in chains adjacent to the Cr atom, respectively. In Fig. 1, the Cl-Cl<sub>(1)</sub> bonds are drawn as solid lines, the Cr-Cl<sub>(2)</sub> bonds as dashed lines. We see from Table II that the AFM values, calculated within PW91, match very well to experimental results, only the elongated octahedron bond length Cr-Cl<sub>(2)</sub> is significantly overestimated—as expected because of the elongated theoretical  $a$  and  $b$  lattice constants.

TABLE II. Internal coordinates of  $\alpha$ -CrCl<sub>2</sub>: 4g Wyckhoff parameters  $x$  and  $y$ ; intra- and interchain Cr-Cl bond lengths in Å; octahedral distortion angle  $\delta$ .

	$x$	$y$	$d(\text{Cr-Cl}_{(1)})$	$d(\text{Cr-Cl}_{(2)})$	$\delta$
Tracy <i>et al.</i> <sup>a</sup>	0.362	0.274	2.40	2.91	0.15°
Oswald <sup>b</sup>	0.362	0.278	2.37	2.91	0.13°
FM, DFT-PW91	0.370	0.290	2.36	3.19	0.29°
FM, DFT-LSDA	0.350	0.263	2.32	2.59	0.04°
AFM, DFT-PW91	0.364	0.287	2.36	3.13	0.11°
AFM, DFT-LSDA	0.339	0.266	2.34	2.55	0.46°

<sup>a</sup>Reference 20.

<sup>b</sup>Reference 19.

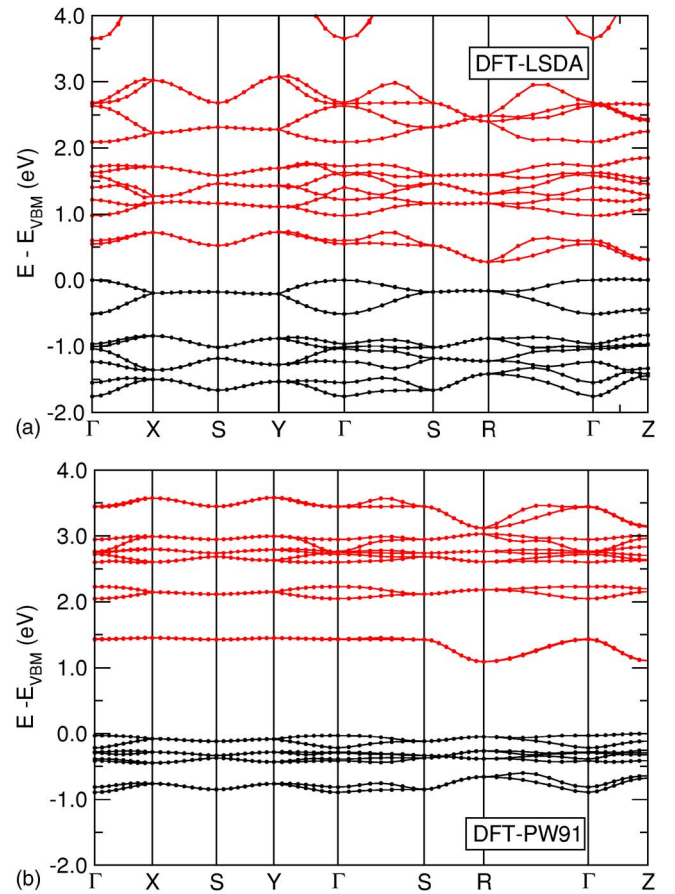


FIG. 3. (Color online) Theoretical band structure of  $\alpha$ -CrCl<sub>2</sub> in DFT-LSDA (upper panel) and DFT-PW91 (lower panel). Black (red/gray) lines denote occupied (empty) energy bands. Energies are normalized to respective valence band maxima.

#### IV. ELECTRONIC PROPERTIES

For the electronic band structure of  $\alpha$ -CrCl<sub>2</sub>, both for the LSDA and PW91 optimized structures, see Fig. 3. Although qualitatively similar, both band structures show quantitative differences. Both methods predict  $\alpha$ -CrCl<sub>2</sub> to be a direct semiconductor whose fundamental band gap is located at  $Z = (0, 0, \frac{1}{2})$  in the BZ. The LSDA band gap is  $E_g = 0.30$  eV, the PW91 band gap is significantly larger, about  $E_g = 1.10$  eV. Since the LSDA equilibrium structure is much smaller than

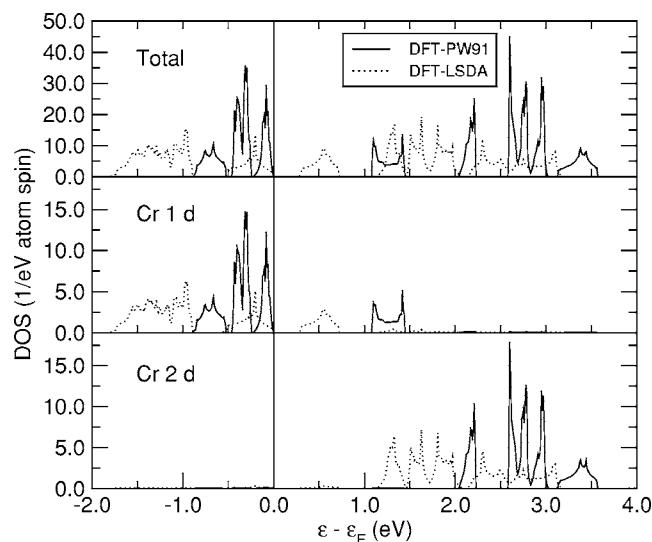


FIG. 4. Electronic density of states (DOS) near the Fermi level  $\varepsilon_F$ . Solid line: DFT-PW91, dotted line: DFT-LSDA. Only one spin component is shown.

in experiment, we expect the respective electronic structure to overestimate the band dispersion and thus underestimate the band gap significantly. However, this cannot be said for the PW91 results, since the optimized structure is somewhat larger than in experiment. This counterbalances to some extent the common DFT band gap underestimation: at the experimental geometry, the band gap is  $E_g=0.80$  eV (0.72 eV) using PW91 (LSDA). The respective band structures (not shown here) are similar to the DFT-PW91 band structure in Fig. 3. Thus, geometrical effects rather than different functionals are responsible for the differences in the band structures.

Both band structures are spin degenerated, as expected from geometrical symmetry reasons. The eight highest occupied bands and the twelve lowest unoccupied bands are Cr 3d bands. Their degeneracy is lifted due to ligand field effects. In LSDA, the bands show dispersion along all crystallographic axes. In PW91, the bands are mostly localized along the crystallographic  $x$  and  $y$  directions, showing only weak interaction. More interaction is found along  $z$ , along the Cr chains.

See Fig. 4 for plots of the corresponding electronic density of states (DOS). They show the total DOS together with the spatially resolved DOS of  $d$  states of adjacent Cr atoms within one chain. As expected they are coupled antiferromagnetically, so the 3d electrons occupy complementary spin states. The bandwidth of the occupied  $d$  bands is about 1.0 eV (1.8 eV) using PW91 (LSDA). The total  $d$ -band splitting is about 4.6 eV (4.8 eV) using PW91 (LSDA). At the experimental geometry, the total splitting is 4.5 eV (4.4 eV) using PW91 (LSDA). It is much less sensitive to the detailed geometry than the band gap  $E_g$ .

We calculate the optical absorption spectrum (Fig. 5) of the AFM crystal within the independent particle approximation.<sup>29</sup> The BZ integration is performed using 512 random  $\mathbf{k}$  points in the BZ. We apply a scissors operator shift of  $\Delta E=0.35$  eV to correct for the DFT band gap

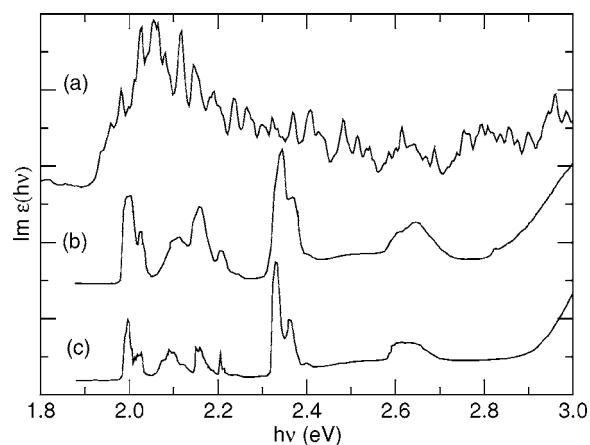


FIG. 5. Optical absorption spectrum of  $\alpha$ -CrCl<sub>2</sub>. (a) Theory: DFT-PW91, with scissors shift of 0.35 eV; (b) Experiment: Bellitto *et al.*;<sup>31</sup> (c) Experiment: Rosseinsky *et al.*<sup>32</sup>

underestimation.<sup>30</sup> Thus, the onset of absorption at about 2.0 eV is comparable with experimental data.<sup>31,32</sup> However, we cannot link the experimentally resolved peaks to specific theoretical transitions. In fact, the agreement with the experimental spectrum is rather poor. This may be due to a poor description of the localized  $d$  electrons. It would be desirable to include the electron self-energy (e.g., within the GW approximation<sup>33</sup>) in the one-particle calculations and electron-hole correlation in the optical spectrum (by solving the corresponding Bethe-Salpeter equation for the polarization function<sup>34</sup>). Both methods have proven useful in the description of transition metal compounds.<sup>35–38</sup> This approach is, however, beyond the scope of this paper. We conclude, however, that DFT calculations underestimate the  $\alpha$ -CrCl<sub>2</sub> band gap by about 0.35 eV. We stress that we include only spin allowed, i.e., singlet transitions in our calculations. Thus the interpretation of the low intensity of the experimental data<sup>31,32</sup> as due to spin-forbidden transitions appears to be incorrect.

Which transitions are responsible for the various peaks? We decompose the optical spectrum with respect to the conduction bands involved. We find that the lowest four conduction bands are responsible for the entire spectrum in the investigated energy range, see upper panel of Fig. 6. Note that only the lowest two conduction bands are localized at the same Cr atom as the valence  $d$  bands of equal spin are (see Fig. 4); the higher conduction  $d$  bands are localized at the nearest neighbor Cr atoms within the same chain. We find that onsite excitations into the lowest conduction band have small transition matrix elements, see lower panel of Fig. 6. Most of the calculated transition peaks are due to interatomic Cr-Cr  $dd$  excitations. They are dipole allowed (as the orbitals are localized on different centers), however, their transition matrix elements are relatively small due to small spatial overlap. This might have led to their wrong assignment as spin-forbidden transitions.

## V. MAGNETIC PROPERTIES

We have found  $\alpha$ -CrCl<sub>2</sub> to be a  $S=2$  Heisenberg antiferromagnet. Due to its chainlike internal structure it should be

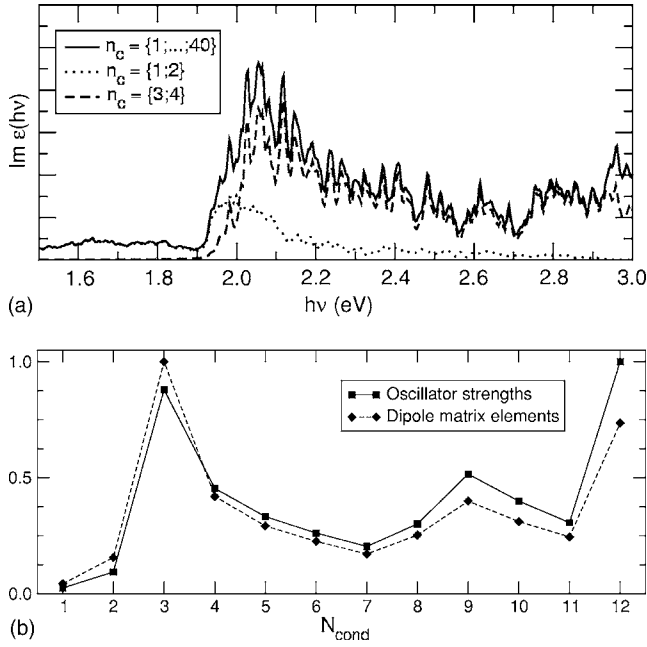


FIG. 6. Upper panel: Conduction band-resolved absorption spectrum of AFM  $\alpha$ -CrCl<sub>2</sub>. Solid line: total absorption spectrum; dotted line: transitions limited to conduction bands 1,2; dashed line: transitions limited to conduction bands 3,4. Lower panel: Conduction band-resolved relative oscillator strengths and dipole matrix elements involving valence  $d$  bands only.

well described by the Heisenberg Hamiltonian

$$H_H = -2J \sum_{c,i} \vec{S}_i \vec{S}_{i+1} - 2J' \sum_{c,i} \sum_{c',i'} \vec{S}_i \vec{S}_{i'}, \quad (1)$$

taking into account intra- and interchain next neighbor coupling. The first sum in (1) runs over all spins  $i$  in each chain  $c$ , the second sum runs over all spins in adjacent chains  $c, c'$ . As usual for spin-unrestricted methods such as UHF or DFT, all solutions apart from the high-spin FM state are no eigenfunctions of  $H_H$ .<sup>39</sup> Instead, we have to work with the Ising Hamiltonian

$$H_I = -2J \sum_{c,i} S_{z,i} S_{z,i+1} - 2J' \sum_{c,i} \sum_{c',i'} S_{z,i} S_{z',i'}, \quad (2)$$

and fit the *first-principles* energies for three different magnetic coupling schemes to respective expectation values of  $H_I$  to obtain  $J$  and  $J'$ . See Fig. 7 for the FM, AFM-I, and AFM-II magnetic couplings that we choose. AFM-I is the magnetic ground state. For these states we have from Eq. (2) the energies

$$E_{\text{FM}} = -2JS^2 + 8J'S^2 + E_0, \quad (3)$$

$$E_{\text{AFM-I}} = 2JS^2 + E_0, \quad (4)$$

$$E_{\text{AFM-II}} = -4J'S^2 + E_0 \quad (5)$$

per spin  $S_i$ , where we also have introduced the nonmagnetic contributions  $E_0$  to the binding energy. Thus, we obtain  $J$  and  $J'$  by

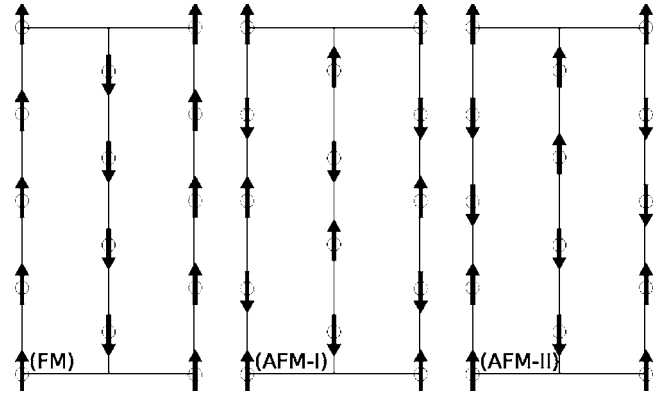


FIG. 7. Sketch of different magnetic cells for calculation of  $J, J'$ : spin orientation of Cr atoms. Chains are aligned vertically.

$$J = \frac{1}{8S^2} (-E_{\text{FM}} + 3E_{\text{AFM-I}} - 2E_{\text{AFM-II}}), \quad (6)$$

$$J' = \frac{1}{16S^2} (E_{\text{FM}} + E_{\text{AFM-I}} - 2E_{\text{AFM-II}}). \quad (7)$$

We calculate  $E_{\text{FM}}, E_{\text{AFM-I}},$  and  $E_{\text{AFM-II}}$  using the experimental cell coordinates and also using the respective optimized structures. The results are given in Table III, and compared to experimental data.<sup>28</sup> At the experimental geometry, we also utilized the PBE exchange-correlation functional<sup>9</sup> and the combination of LSDA with onsite Coulomb repulsion terms (LSDA+U).<sup>2</sup> We chose  $U+J=3.8$  eV in the LSDA+U theory, which gave the best agreement for the  $J$  coupling constant. For all methods, we reproduce the antiferromagnetic character of  $\alpha$ -CrCl<sub>2</sub>, i.e.,  $J < 0$ . We also find  $J' > 0$  and  $|J'| \ll |J|$  and the  $J'/J$  ratio in quite good agreement with experiment. However, apart from the intentionally fitted LSDA+U result, all functionals overestimate the antiferromagnetic coupling  $J$  by at least a factor of two, and perform even worse for the interchain coupling  $J'$ . Using the optimized geometries for the PW91 and LSDA calculations gives no improvements for the results. We note that the PW91 results are very similar to those obtained at the experimental geometry. Indeed, we find  $J \approx -20$   $k_B/K$ ,  $J' \approx 2 \cdot \cdot 3$   $k_B/K$  over a large variation of the cell volume per

TABLE III. Spin coupling constants in  $\alpha$ -CrCl<sub>2</sub>, calculated at experimental and theoretical geometries by various methods.

		$J(k_B/K)$	$J'(k_B/K)$	$J'/J$
	Winkelmann <i>et al.</i> <sup>a</sup>	-9.5	1.23	-0.13
Experimental	LSDA	-23.9	2.68	-0.11
	Geometry			
Optimized	PW91	-19.4	3.08	-0.16
	PBE	-18.0	3.62	-0.20
	PBE0	-37.9	-11.19	0.30
	LSDA+U	-9.6	1.46	-0.15
Optimized	LSDA	-49.5	4.32	-0.09
	Geometry			
	PW91	-19.8	3.08	-0.16

<sup>a</sup>Reference 28.

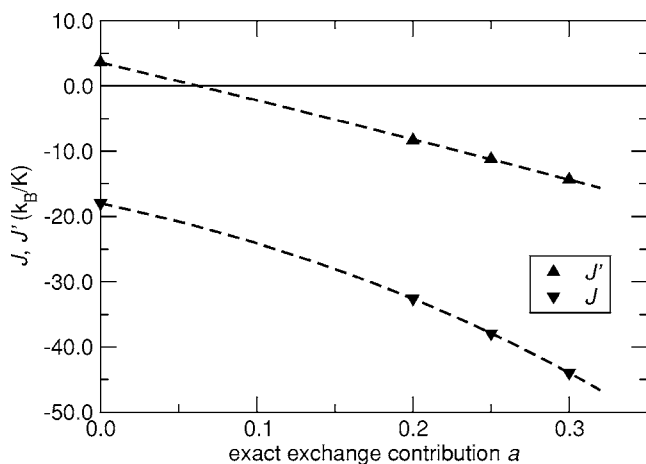


FIG. 8. Magnetic coupling constants  $J$ ,  $J'$  from hybrid-DFT calculations, varying the exact exchange mixing coefficient  $a$ .

$\text{CrCl}_2$  unit ( $\Omega_0=75\cdots 95 \text{ \AA}^3$ ). The reason is almost parallel energy surfaces for the different magnetic couplings (see lower panel of Fig. 2 for FM, AFM-I energy surfaces).

It is a well-known shortcoming of DFT to describe the interaction in strongly correlated systems wrong.<sup>40,41</sup> This deficiency can be partially overcome by explicitly correcting for the electronic self-interaction<sup>42,43</sup> or including to some extent exact exchange in the exchange-correlation functional.<sup>44</sup> Recently, Perdew *et al.* argued for an exact exchange mixing coefficient  $a=0.25$  from coupling-constant integration<sup>5</sup> and the according extension (“PBE0”) of the PBE exchange-correlation functional<sup>45</sup> has given improved magnetic coupling parameters.<sup>46</sup> We perform exact exchange calculations with variable mixing coefficient  $a$  around  $a=0.25$ ; see Fig. 8 for the results. A strong dependence of  $J$  and  $J'$  on the value of  $a$  can be stated, however, in contrast to other studies including exact exchange does not improve the

agreement with experimental data. Both  $J$  and  $J'$  are negative around  $a=0.25$ , suggesting an antiferromagnetic interchain coupling and thus a positive ratio  $J'/J$ , in contrast to experiment.

## VI. CONCLUSIONS

In summary, we have investigated the transition metal-halide  $\alpha\text{-CrCl}_2$  using *first-principles* DFT calculations. We have optimized the crystal structure utilizing the LSDA and PW91 exchange-correlation functionals. We confirm experimental data that  $\alpha\text{-CrCl}_2$  is anti-ferromagnetically coupled within the chains along the  $c$  axis. The PW91 optimized structure shows good agreement with experiment. The independent-particle singlet optical spectrum, including a scissors operator shift of  $\Delta E=0.35 \text{ eV}$ , does not agree very well with experiment. This should be largely due to the poor description of the energetic positions of the localized  $d$  electrons. We attribute the peaks in the energy region  $h\nu=2\cdots 3 \text{ eV}$  to Cr  $d$ -transitions between neighboring Cr atoms. The intra- and interchain magnetic coupling constants are calculated using various methods; all local and semilocal exchange-correlation descriptions grossly overestimate the magnetic coupling. A LSDA+U study with  $U+J=3.8 \text{ eV}$  gives good agreement with experiment. Hybrid DFT calculations (which include to some extent the exact exchange operator) give rather poor results with a qualitatively different interchain coupling scheme.

## ACKNOWLEDGMENTS

We thank M. Hargittai for useful discussions. Generous grants of computer time from the High Performance Computing Committee of Massey University and the Höchstleistungsrechenzentrum Stuttgart are gratefully acknowledged.

\*Electronic address: a.h.hermann@massey.ac.nz

†Electronic address: p.a.schwertdfeger@massey.ac.nz

<sup>1</sup>J. P. Perdew and A. Zunger, Phys. Rev. B **23**, 5048 (1981).

<sup>2</sup>V. I. Anisimov, J. Zaanen, and O. K. Andersen, Phys. Rev. B **44**, 943 (1991).

<sup>3</sup>F. Ortman, F. Bechstedt, and W. G. Schmidt, Phys. Rev. B **73**, 205101 (2006).

<sup>4</sup>A. D. Becke, J. Chem. Phys. **98**, 1372 (1993).

<sup>5</sup>J. P. Perdew, M. Ernzerhof, and K. Burke, J. Chem. Phys. **105**, 9982 (1996).

<sup>6</sup>T. Kotani, Phys. Rev. Lett. **74**, 2989 (1995).

<sup>7</sup>M. Städele, J. A. Majewski, P. Vogl, and A. Görling, Phys. Rev. Lett. **79**, 2089 (1997).

<sup>8</sup>J. P. Perdew, J. A. Chevary, S. H. Vosko, K. A. Jackson, M. R. Pederson, D. J. Singh, and C. Fiolhais, Phys. Rev. B **46**, 6671 (1992).

<sup>9</sup>J. P. Perdew, K. Burke, and M. Ernzerhof, Phys. Rev. Lett. **77**, 3865 (1996).

<sup>10</sup>M. Hargittai, Chem. Rev. (Washington, D.C.) **100**, 2233 (2000).

<sup>11</sup>M. E. Jacox and D. E. Milligan, J. Chem. Phys. **51**, 4143 (1969).

<sup>12</sup>J. S. Ogden and R. S. Wyatt, J. Chem. Soc. Dalton Trans. **1987**, 859.

<sup>13</sup>V. R. Jensen, Mol. Phys. **91**, 131 (1997).

<sup>14</sup>S. G. Wang and W. H. E. Schwarz, J. Chem. Phys. **109**, 7252 (1998).

<sup>15</sup>A. J. Bridgeman and C. H. Bridgeman, Chem. Phys. Lett. **272**, 173 (1997).

<sup>16</sup>I. M. B. Nielsen and M. D. Allendorf, J. Phys. Chem. A **109**, 928 (2005).

<sup>17</sup>N. Schiefenhövel, M. Binnewies, F. Janetzko, and K. Jug, Z. Anorg. Allg. Chem. **627**, 1513 (2001).

<sup>18</sup>S. Smith and I. H. Hillier, J. Chem. Soc., Chem. Commun. **1989**, 539.

<sup>19</sup>H. R. Oswald, Helv. Chim. Acta **44**, 1049 (1961).

<sup>20</sup>J. W. Tracy, N. W. Gregory, E. C. Lingafelter, J. D. Dunitz, H.-C. Mez, R. E. Rundle, C. Scheringer, H. L. Y. Jnr, and M. K. Wilkinson, Acta Crystallogr. **14**, 927 (1961).

<sup>21</sup>G. Kresse and J. Furthmüller, Phys. Rev. B **54**, 11169 (1996).

<sup>22</sup>P. Hohenberg and W. Kohn, Phys. Rev. **136**, B864 (1964).

<sup>23</sup>U. von Barth and L. Hedin, J. Phys. C **5**, 1629 (1972).

- <sup>24</sup>P. E. Blöchl, Phys. Rev. B **50**, 17953 (1994).
- <sup>25</sup>G. Kresse and D. Joubert, Phys. Rev. B **59**, 1758 (1999).
- <sup>26</sup>P. Vinet, J. Ferrante, J. R. Smith, and J. H. Rose, J. Phys. C **19**, L467 (1986).
- <sup>27</sup>M. Hagiwara and K. Katsumata, J. Magn. Magn. Mater. **140**, 1665 (1995).
- <sup>28</sup>M. Winkelmann, M. Baehr, M. Reehuis, M. Steiner, M. Hagiwara, and K. Katsumata, J. Phys. Chem. Solids **58**, 481 (1997).
- <sup>29</sup>H. Ehrenreich and M. H. Cohen, Phys. Rev. **115**, 786 (1959).
- <sup>30</sup>R. Del Sole and R. Girlanda, Phys. Rev. B **48**, 11789 (1993).
- <sup>31</sup>C. Bellitto, H. Brunner, and H. Guedel, Inorg. Chem. **26**, 2750 (1987).
- <sup>32</sup>D. R. Rosseinsky and I. A. Dorrity, J. Phys. Chem. **81**, 26 (1977).
- <sup>33</sup>L. Hedin, Phys. Rev. **139**, A796 (1965).
- <sup>34</sup>W. G. Schmidt, S. Glutsch, P. H. Hahn, and F. Bechstedt, Phys. Rev. B **67**, 085307 (2003).
- <sup>35</sup>S. Massidda, A. Continenza, M. Posternak, and A. Baldereschi, Phys. Rev. Lett. **74**, 2323 (1995).
- <sup>36</sup>F. Aryasetiawan and O. Gunnarsson, Phys. Rev. Lett. **74**, 3221 (1995).
- <sup>37</sup>N.-P. Wang, M. Rohlfing, P. Krüger, and J. Pollmann, Phys. Rev. B **71**, 045407 (2005).
- <sup>38</sup>R. Laskowski and N. E. Christensen, Phys. Rev. B **73**, 045201 (2006).
- <sup>39</sup>L. Noodleman, J. Chem. Phys. **74**, 5737 (1981).
- <sup>40</sup>R. L. Martin and F. Illas, Phys. Rev. Lett. **79**, 1539 (1997).
- <sup>41</sup>J. N. Harvey, Structure and Bonding **112**, 151 (2004).
- <sup>42</sup>A. Svane and O. Gunnarsson, Phys. Rev. Lett. **65**, 1148 (1990).
- <sup>43</sup>S. L. Dudarev, G. A. Botton, S. Y. Savrasov, Z. Szotek, W. M. Temmerman, and A. P. Sutton, Phys. Status Solidi A **166**, 429 (1998).
- <sup>44</sup>A. D. Becke, J. Chem. Phys. **104**, 1040 (1996).
- <sup>45</sup>C. Adamo and V. Barone, J. Chem. Phys. **110**, 6158 (1999).
- <sup>46</sup>C. Franchini, V. Bayer, R. Podloucky, J. Paier, and G. Kresse, Phys. Rev. B **72**, 045132 (2005).